

Supplementary material for *Global rates of water-column denitrification derived from nitrogen gas measurements*

Tim DeVries,¹ Curtis Deutsch,¹ François Primeau,² Bonnie Chang,³ Allan Devol⁴

¹Department of Atmospheric and Oceanic Sciences, University of California, Los Angeles, CA 90095 USA

²Department of Earth System Science, University of California, Irvine, CA 92697 USA

³Department of Geosciences, Princeton University, Princeton, NJ 08544 USA

⁴School of Oceanography, University of Washington, Seattle, WA 98195 USA

1 Supplementary Methods

Data-constrained ocean circulation model The ocean circulation model is based on the inverse model of ref. 1 and is fit to climatological potential temperature, salinity, and natural radiocarbon distributions, as well as climatological mean sea-surface height, sea-surface heat fluxes, and sea-surface freshwater fluxes. Here we have extended this work by increasing the model resolution to 2 degrees in the horizontal, and by adding CFC-11 bottle data from the Global Ocean Data Analysis Project (GLODAP)² to constrain the circulation model. CFC-11 is modeled following the OCMIP-2 protocols³. The air-sea

flux for CFCs is computed by

$$F = K_w(C_{sat} - C_s) \quad (1)$$

where C_{sat} is the time-dependent saturation surface concentration for CFC-11, and C_s is the modeled surface concentration. The piston velocity K_w is derived from climatological wind stress fields⁴ and reduced by the fractional extent of sea ice cover. A one-year time step is used for the CFC-11 simulation, starting in 1938 and ending in 1998.

We used an adjoint method to adjust the circulation and air-sea fluxes in order to minimize the model-data misfit (see ref. 1 for details). At the optimal solution, the normalized model-data misfit is 1.2 for potential temperature, 1.0 for salinity, 0.5 for natural radiocarbon, 2.2 for CFC-11, 1.1 for sea-surface height, 0.4 for sea-surface heat flux, and 0.3 for sea-surface freshwater flux. (A normalized model-data misfit of 1 indicates that the model-data residuals are distributed with the same covariance as the data errors). The normalized model-data residuals for CFC-11 are higher than for the other tracers, but the globally-averaged rms model-data misfit is still quite small at $0.20 \text{ pmol kg}^{-1}$, which is about the same as that achieved by a previous global inverse model⁵. Importantly for this project, the fit to CFCs is very good in the suboxic zones (defined in Figure 1). The rms misfit is only $0.05 \text{ pmol kg}^{-1}$ in the Arabian Sea, $0.08 \text{ pmol kg}^{-1}$ in the ETSP, and $0.06 \text{ pmol kg}^{-1}$ in the ETNP (Supplementary Figure 1). Near the locations where there is N_{xs}

data, depth profiles of modeled and observed CFC-11 concentrations display a very tight match (Supplementary Figure 1). Plots of modeled and observed CFC-11 concentrations along transects through the suboxic zones are displayed in Supplementary Figure 2.

Excess nitrogen gas simulations N_{xs} is modeled with a source in the water column where the observed oxygen concentration falls below a critical threshold,

$$\Gamma_{xs} = r_{N:C_{org}}^i \times \Gamma_{org} \quad iff \quad O_{2,obs} < O_{2,crit}^i \quad (2)$$

where Γ_{xs} is the production rate of N_{xs} ($\mu\text{M N yr}^{-1}$), Γ_{org} is the remineralization rate of organic carbon ($\mu\text{M C yr}^{-1}$), $r_{N:C_{org}}$ is a stoichiometric proportionality constant (mol N (mol C) $^{-1}$), and $O_{2,crit}$ is the critical oxygen threshold. The index i differentiates the three suboxic zones (Arabian Sea, ETSP, or ETNP). The proportionality constant $r_{N:C_{org}}$, representing the number of moles N produced in the form of N_2 gas during microbial respiration of 1 mol of organic carbon (C_{org}) under suboxic conditions, is allowed to vary from one suboxic zone to another, as is the critical oxygen threshold $O_{2,crit}$. This is necessary because the composition of microbial communities may vary widely from one region to another^{6,7}.

The observed oxygen concentration $O_{2,obs}$ is derived from the 2009 World Ocean Atlas (WOA09) climatology⁸. We apply the empirical correction suggested by ref. 9 to the monthly gridded WOA09 O_2 maps, which produces a better representation of the total vol-

ume of suboxic waters in the ocean, and a better match to high-quality data from the World Ocean Circulation Experiment (WOCE) in the suboxic zones. The extent of the suboxic zone within each OMZ is then determined using a hyperbolic tangent transformation,

$$\eta = .5 \times (1 - \tanh(\mathbf{O}_{2,obs} - \mathbf{O}_{2,crit}^i)) \quad (3)$$

so that areas within the permanent suboxic zone receive a value of 1, and areas where suboxia never occurs receive a value of 0. This mask is then time-averaged and interpolated to the model grid to determine the extent of the suboxic zones in the model. (The gray shading in Figure 1 shows the depth-maximum value of η , after interpolation to the model grid, for the case that $\mathbf{O}_{2,crit}$ is 5 μM in all three suboxic zones). This η then replaces the “if” statement in equation (2) so that the production of \mathbf{N}_{xs} becomes

$$\Gamma_{xs} = r_{N:C_{org}}^i \times \eta \times \Gamma_{org}. \quad (4)$$

The organic matter remineralization rate is parameterized with a power-law dependence on depth¹⁰

$$\Gamma_{org} = \frac{\partial}{\partial z} \left(J_0 \times \left(\frac{z}{z_{eu}} \right)^{-b^i} \right), \quad (5)$$

where J_0 is the rate of export of organic carbon at the base of the euphotic zone z_{eu} (considered to be the top 2 layers in the model, to the depth $z_{eu} = 73$ m), and the attenuation coefficient b is allowed to vary from one suboxic zone to another to reflect differences in

how rapidly the rate of organic matter oxidation decreases with depth. The carbon export rate J_0 is calculated from satellite-based estimates of net primary production (NPP),

$$J_0 = \phi_{ex} \times \text{NPP}, \quad (6)$$

where the export ratio ϕ_{ex} is an empirically-determined function of NPP and temperature ¹¹. Uncertainty in the rate of net primary production is taken into account by using three different satellite-based NPP algorithms, each of which is based on SeaWiFS data for the period 1998-2007. The algorithms used to produce the NPP estimates are the standard vertically generalized production model (VGPM) ¹², the Eppley variant of the VGPM ¹², and the carbon-based productivity model ¹³. The NPP fields used here are the average of the monthly fields for the period 1998-2007.

The only sink of N_{xs} is due to gas exchange with a well-mixed atmosphere ($N_{xs}^{atm} = 0$) at a piston velocity of 3 m d^{-1} .

Markov chain Monte Carlo simulations The uncertain control parameters in the above parameterization are $r_{N:C_{org}}^i$, $O_{2,crit}^i$, and b^i . Each control parameter is allowed to vary independently from one suboxic zone to another, giving a total of nine (3×3) control parameters. We use a Markov chain Monte Carlo (MCMC) approach to sample from the posterior probability density function (pdf) for these model parameters. The target distribution is the product of a likelihood function times a prior pdf for each parameter.

The likelihood function is modeled as a multivariate Gaussian $P(\mathbf{N}_{xs}) \sim N(\mathbf{N}_{xs}^{obs}, \sigma_{N_{xs}}^2)$, where \mathbf{N}_{xs}^{obs} are the observed \mathbf{N}_{xs} concentrations averaged onto the model grid, and $\sigma_{N_{xs}}$ is chosen to be $\max(1\mu\text{M}, 0.1 \times \mathbf{N}_{xs}^{obs})$. When evaluating the likelihood function we average modeled \mathbf{N}_{xs} concentrations onto the grid points for which there is data using a Gaussian averaging filter with a 200 km radius. This averaging is performed in order to minimize the influence of grid-scale noise in the circulation, production, and oxygen fields.

We do not include in our data constraints N_2 gas data from outside the suboxic zones, but assume that the \mathbf{N}_{xs} calculations that were performed on the original N_2/Ar data correctly isolate the effects of water-column denitrification. The original numbers were derived assuming that \mathbf{N}_{xs} at certain reference locations outside the suboxic zones are zero^{14–16}. We checked the \mathbf{N}_{xs} concentrations at these locations and confirmed that they are close to zero. A simulation including the constraint that $\mathbf{N}_{xs}^{obs} = 0$ at the reference locations also found consistency with the data, with only slightly ($\sim 5\%$) lower integrated N loss rates.

The parameter space for the MCMC simulation is defined by the prior pdfs for the model control parameters (Supplementary Figure 3). The prior pdfs represent an estimate of a reasonable range of values for the control parameters, derived from prior knowledge. For the value of the stoichiometric constant $r_{N:C_{org}}$ we choose a prior with a peak proba-

bility near 1, to reflect the fact that about 1 mol N is used per mole C metabolized during denitrification¹⁷. The prior is right-skewed so that the prior probability drops off rapidly for values of $r_{N:C_{org}}$ less than 0.5, and less rapidly for values of $r_{N:C_{org}}$ greater than 2, reaching zero probability by about $r_{N:C_{org}} = 5$. The wide prior for $r_{N:C_{org}}$ accounts for variability in the stoichiometry of organic matter¹⁷ as well as uncertainty in the magnitude of the organic C export rates derived from satellite NPP fields. The prior pdf for the critical oxygen threshold $O_{2,crit}$ has a peak value in the range 3-5 μM (Supplementary Figure 3), reflecting the fact that the critical oxygen threshold for denitrification to occur from a microbial standpoint is around 2-4 μM ¹⁸. The distribution is right-skewed, so that large values of $O_{2,crit}$ are tolerated, up to about 15 μM where the prior probability approaches zero. Including these larger values accounts for the temporal and spatial averaging that goes into creating the mapped data sets, which may necessitate using a larger value of O_2^{crit} that is applicable not at the microbial level but at the large scales of the mapped data sets. The interquartile range for the prior pdf for b is 0.2-2, reflecting the large variability in the efficiency at which organic matter is transferred to depth¹⁹, while the peak value is in the range 0.4-1.0, reflecting the range of values determined for this parameter within low-oxygen zones²⁰⁻²².

The MCMC simulations were carried out by running 18 chains independently (six chains for each of the three different NPP fields), starting with an initial random draw from

an appropriately overdispersed distribution. Each chain used the method of slice sampling²³, as implemented in the MATLAB routine `slicesample.m`, to sample from the posterior pdf. Each chain was run for long enough to produce 5000 samples for each parameter. The potential scale reduction factor²⁴ for the 18 chains was less than 1.1 for each parameter, indicating that the chains had converged to the target distribution. We removed the first 1000 samples from each chain to ensure that the initial condition had been forgotten, and the remaining 72,000 parameter sets (18×4000) were used to calculate the rate of nitrogen loss in each suboxic zone due to water-column denitrification by integrating equation (4) within each suboxic zone.

2 Supplementary Discussion

Posterior distributions of model parameters Supplementary Table 1 summarizes the posterior distributions of the model control parameters determined from the results of the MCMC simulations. The mean value of the stoichiometric coefficient $r_{N:C_{org}}$ is 0.8 in both the Arabian Sea and the ETNP, suggesting canonical denitrification with Redfieldian stoichiometry ($r_{N:C_{org}} \sim 1$) is dominant in these regions. By contrast, the mean value of $r_{N:C_{org}}$ in the ETSP is significantly higher at 2.2. The observed elemental composition of organic matter along with known reaction pathways for N₂ production¹⁷ make such a high value of $r_{N:C_{org}}$ unlikely, indicating that the model is probably choosing a high value

of $r_{N:C_{org}}$ to compensate for an underestimate of the rate of C_{org} export in the ETSP. The mean value of the critical oxygen threshold is about 3-4 μM in all three suboxic zones, consistent with the expected value of 2-4 μM ¹⁸. The mean value of the organic matter attenuation coefficient b is 0.6 in the ETNP, which is in line with existing estimates from that region^{20,21}. The mean values of b in the Arabian Sea and the ETSP (1.3 and 1.2, respectively) are slightly higher than suggested by sediment trap data in these regions²². This could indicate that some organic matter (perhaps smaller particles) remineralizes shallower in the water-column than the bulk organic matter in these regions. If there are such differences, the b values fit here will reflect the organic matter remineralizing shallower in the water-column, where the suboxic zones and N_2 production are concentrated.

An important point is that the total N loss rate in each suboxic zone is relatively insensitive to the values of the model parameters, as shown in Supplementary Figure 4, demonstrating that the N loss rates inferred here are robust over a wide range of parameter-space. In particular, our model does not show the strong sensitivity of integrated denitrification rates to $\text{O}_{2,crit}$ that is shown in other studies^{9,25}. This is because when $\text{O}_{2,crit}$ increases and the volume of suboxic waters expand, the rate of denitrification decreases in order to match the observed N_{xs} concentrations. Thus the constraint provided by the N_{xs} data maintains an inverse relationship between the volume of suboxic waters and the rate of denitrification within the suboxic water column. The greatest sensitivity is found

between the N loss rate in the ETSP and the value of $r_{N:C_{org}}$ ($R^2 = 0.28$). This shows that at the most probable values of $r_{N:C_{org}}$ (around 1), the integrated N loss rate within the ETSP is toward the lower end of its uncertainty estimate.

Sensitivity of integrated N loss rates to ventilation rates and parameterization of organic matter export The concentration of N_{xs} in the suboxic zone is determined by a balance between the rate of production of N_2 gas (which is tied to the rate of organic carbon export and remineralization), and the rate at which the suboxic zone is ventilated. Here we perform several additional experiments to investigate the sensitivity of our approach to estimating integrated N loss rates to the parameterization of organic matter export and remineralization, and to ventilation rates in the suboxic zone.

To explore the sensitivity to the parameterization of organic matter export and remineralization, we simulate export production by coupling an OCMIP-type biogeochemistry model³ to our optimized circulation model (Experiment S1). We use the default production and remineralization parameters given by the OCMIP-2 protocols³, and make no attempt to tune the parameters to achieve consistency with the nutrient or oxygen fields. Nevertheless, the modeled nutrient fields at depths of maximum denitrification ($\sim 150\text{-}350$ m) compare reasonably well to the observations (Supplementary Figure 5). The model also produces suboxic waters in the three main suboxic zones. Greatest differences be-

tween model and observations occur in the Arabian Sea. This may be due to the strong seasonality of export production in this region, which is not captured by the steady circulation model. By re-running the MCMC simulations with Γ_{org} (equation 5) fixed at the value obtained from this model, we obtained an estimate of N loss rates in each suboxic zone that is not conditioned on the satellite NPP fields. The N loss rates obtained from this model agree with those obtained in the standard model in the Arabian Sea and the ETNP, but the rate in the ETSP is significantly lower than in the standard model (Supplementary Table 2). The fit to the N_{xs} data (not shown) is very good in the Arabian Sea and the ETNP, but significantly degraded in the ETSP where the shallow peak is not reached, indicating that the higher rates inferred in the standard model are more probable. The optimal parameter values are slightly different in this simulation than in standard model. Critical oxygen thresholds are uniformly higher, perhaps because the production in the OCMIP model is less concentrated in coastal areas than in the satellite production estimates. Like the standard model, the value of $r_{N:C_{org}}$ in this simulation is higher in the ETSP (2.0) than in the Arabian Sea (1.3) or the ETNP (1.1), which again could indicate that organic carbon export into the suboxic zone is too weak in this region.

To explore the sensitivity to the rate at which the suboxic zone is ventilated we performed two experiments, one in which we doubled the horizontal diffusivity from $1000\text{ m}^2\text{ s}^{-1}$ to $2000\text{ m}^2\text{ s}^{-1}$ (Experiment S2), and one in which we doubled the vertical diffusivity

from 10^{-5} m 2 s $^{-1}$ to 2×10^{-5} m 2 s $^{-1}$ (Experiment S3). We maintain the satellite-based export production rates from the standard model, and repeat the MCMC simulations with the more diffusive transport. (Here we use only the VGPM NPP estimates, as our results showed little sensitivity to the algorithm used to determine NPP). The results show an increase in the rate of N loss needed to match the N_{xs} observations in each of the suboxic zones (Supplementary Table 2). This is due to the fact that with enhanced diffusion, the suboxic zones are better ventilated as a whole, and less N_{xs} accumulates in the suboxic zone per unit production. This demonstrates the importance of correctly simulating ventilation rates in the suboxic zones. To the degree that the ventilation rates in the suboxic zones can be constrained by the available radiocarbon and CFC-11 data, the data-constrained circulation model used here can be expected to have accurate ventilation rates in the suboxic zones. By contrast, the suboxic zones of experiments S2 and S3 are too well ventilated, as indicated by increased CFC-11 concentrations within these zones. In comparison to the standard model, Experiment S2 has 7% higher CFC concentrations in the Arabian Sea, 80% higher in the ETSP, and 33% higher in the ETNP, while Experiment S3 has 25% higher CFC concentrations in the Arabian Sea, 75% higher in the ETSP, and 60% higher in the ETNP.

Comparing modeled denitrification rates with those estimated by geochemical methods The rates of denitrification estimated here are lower, especially in the Arabian Sea,

than most other previous estimates. To explain the disparity between all of the various estimates is beyond the scope of this study. However, we did apply two simple “geochemical” methods for estimating denitrification to the model-simulated N_{xs} “data”, to see if the modeled rates could be reproduced. (By geochemical methods we mean methods that calculate average volumetric rates and extrapolate over the entire suboxic zone to get the integrated N loss). Our goal is not to reproduce the exact methods used in previous papers, but merely to explore to what extent there might be differences between the rates predicted by the 3-d circulation model used here and more simplified geochemical models that consider only average rates and do not take into account all of the mixing effects present in and around the suboxic zones.

We used two independent approaches to attempt to reconstruct the known denitrification rates in the model using model-simulated N_{xs} concentrations and age tracers as artificial observations. In the first method, which we refer to as the “averaging method”, we calculated an average denitrification rate by dividing the average N_{xs} concentration in the suboxic zone (after applying a simple correction based on the correlation between temperature and N_{xs} outside the suboxic zone to account for mixing effects²⁶) by the average age (or replacement time) of waters in the suboxic zone. In the second method, which we refer to as the “regression method”, we estimated the average rate of denitrification in each suboxic zone by the slope of a linear regression of N_{xs} against age within each suboxic

zone²⁷. In each case, the estimated average rate is then multiplied by the total volume of suboxic waters to produce the integrated rate of denitrification within each suboxic zone. The total volume of suboxic waters is assumed to be the volume wherein $\eta > 0.01$ (see equation (4)). We calculated the replacement time of waters in the suboxic zone with an ideal age tracer that has an age of 0 years everywhere outside the suboxic zone, and that ages at a rate of 1 year per year within the suboxic zone. The average age of suboxic waters calculated in this way is 3.9 ± 0.5 years in the Arabian Sea, 0.9 ± 0.4 years in the ETSP, and 3.9 ± 0.8 years in the ETNP.

Supplementary Figure 6 shows the denitrification rates calculated by applying the above two geochemical methods to model-simulated N_{xs} “data” from the Arabian Sea region. The simulated data used here are results from 500 model runs, drawn randomly from one of the MCMC simulations used to fit the model-simulated N_{xs} concentrations to the observations. The difference between denitrification rates estimated with the averaging method and the modeled denitrification rates amounts to 9 ± 2 Tg N yr⁻¹, displaying a significant positive bias and moderate scatter. The difference between denitrification rates estimated with the regression method and the model is 13 ± 9 Tg N yr⁻¹, displaying an even larger bias and scatter than the averaging method.

To isolate potential sources of bias in the averaging method and the regression

method, we performed a series of five idealized model experiments (Supplementary Table 3). In each experiment the suboxic zone is defined by $O_{2,crit} = 4 \mu M$ in the Arabian Sea. As above, the suboxic volume for geochemical rate estimates is the volume in which $\eta > 0.01$. The volumetric rate of N_{xs} production ($r_{N:C_{org}}$) is tuned to yield an integrated N loss of 13.0 TgN yr^{-1} in the Arabian Sea. In Experiment 1, we set the rate of production of N_2 to be uniform everywhere within the suboxic zone, and we use a boundary condition of zero N_{xs} concentration outside the suboxic zone. Table S2 shows that these are sufficient conditions for the averaging method and the regression method to both yield the correct rate of N loss. However, these conditions are not likely to be met in the real ocean. In reality, the rate of denitrification is spatially variable due to variability in the rate of organic matter remineralization and in the in-situ oxygen concentration. Likewise, N_{xs} concentrations do not drop to zero outside of the suboxic zone due to circulation processes that mix N_{xs} into waters outside the suboxic zone.

In Experiment 2, we retain uniform rates of N_2 production in the suboxic zone, but allow ocean currents to mix tracer outside the suboxic zone as it would in the real ocean. In this case the rates estimated with both the averaging method and the regression method are larger than the modeled rates. This shows that the regression between temperature and N_{xs} that we used to correct for mixing effects in the averaging method²⁶ does not fully account for mixing of tracer from off the boundary into the suboxic zone. We think the

source of positive bias in the regression method arises along the edges of the suboxic zone where the age approaches zero but the N_{xs} concentration is non-zero. Because the age approaches zero more rapidly toward the edges of the suboxic zone than does the tracer concentration, these points near the edges of the suboxic zone bias the linear fit toward too large reaction rates. However, it is not clear if this relationship would hold if CFC ages were used, as is typical of most geochemical methods²⁷.

In Experiments 3 and 4 we retain the uniform (zero) tracer boundary condition from Experiment 1, but allow the rate of production of N_{xs} to vary spatially within the suboxic zone. In Experiment 3, the production rate varies with depth by tying the production rate to an organic matter remineralization profile (equation (5)) with exponent $b = 1$. In this case the rates estimated with the averaging method and the regression method are biased low. By contrast, in Experiment 4 the production rate is varied by multiplying the production rate by η (equation (3)), which is approximately the proportion of time (months out of the year) that the O_2 concentration falls below $4\mu M$. In this case the rates estimated with the geochemical methods are biased high. We believe that the biases in these cases are due to how the production of N_{xs} is distributed in relation to the core of the suboxic zone. A simple spherical reaction-diffusion model showed that both the averaging method and the regression method underestimate (overestimate) rates when the reaction rate decreases (increases) toward the center of the sphere. To the degree that this relationship holds in the

real ocean we would expect a negative bias from these methods when peak denitrification rates occur at the edge of the suboxic zone, and a positive bias when peak denitrification rates occur at the center of the suboxic zone. When the production is distributed according to an organic matter flux profile (Experiment 3), peak production rates occur at shallower depths than the core of the suboxic zone. When the production scales with η (Experiment 4), production rates increase toward the core of the suboxic zone. In reality both effects are present, and the magnitude of the bias depends on how attenuated the organic matter flux is and on how concentrated the core of the suboxic zone is.

Experiment 5 uses both realistic (non-uniform) tracer boundary conditions and production rates that are calculated using the full model described above (equation (4)). In this case, the biases identified here combine to produce an overestimate of N loss with both the averaging method and the regression method.

The methods used here were not meant to be exact replications of previous studies using geochemical methods, but were meant to illustrate some of the potential problems when estimating integrated rates using bulk averages of spatially variable processes. Thus the results shown here do not disprove previous rate estimates, but they do demonstrate a potentially large degree of uncertainty in such estimates, as well as potential for bias to higher rates. We also note that significant sources of uncertainty, such as the age of waters

in the suboxic zone and the volume of suboxic waters, are eliminated in the present context since these are known from the model output. In reality, the volume of suboxic waters is typically based on various *ad hoc* assumptions^{14,26–28}, and the age of suboxic waters is typically estimated from CFC concentrations^{27,28} or a range is taken from previously published estimates²⁶. When error from these sources is considered, the imprecision of the geochemical methods may be further exacerbated.

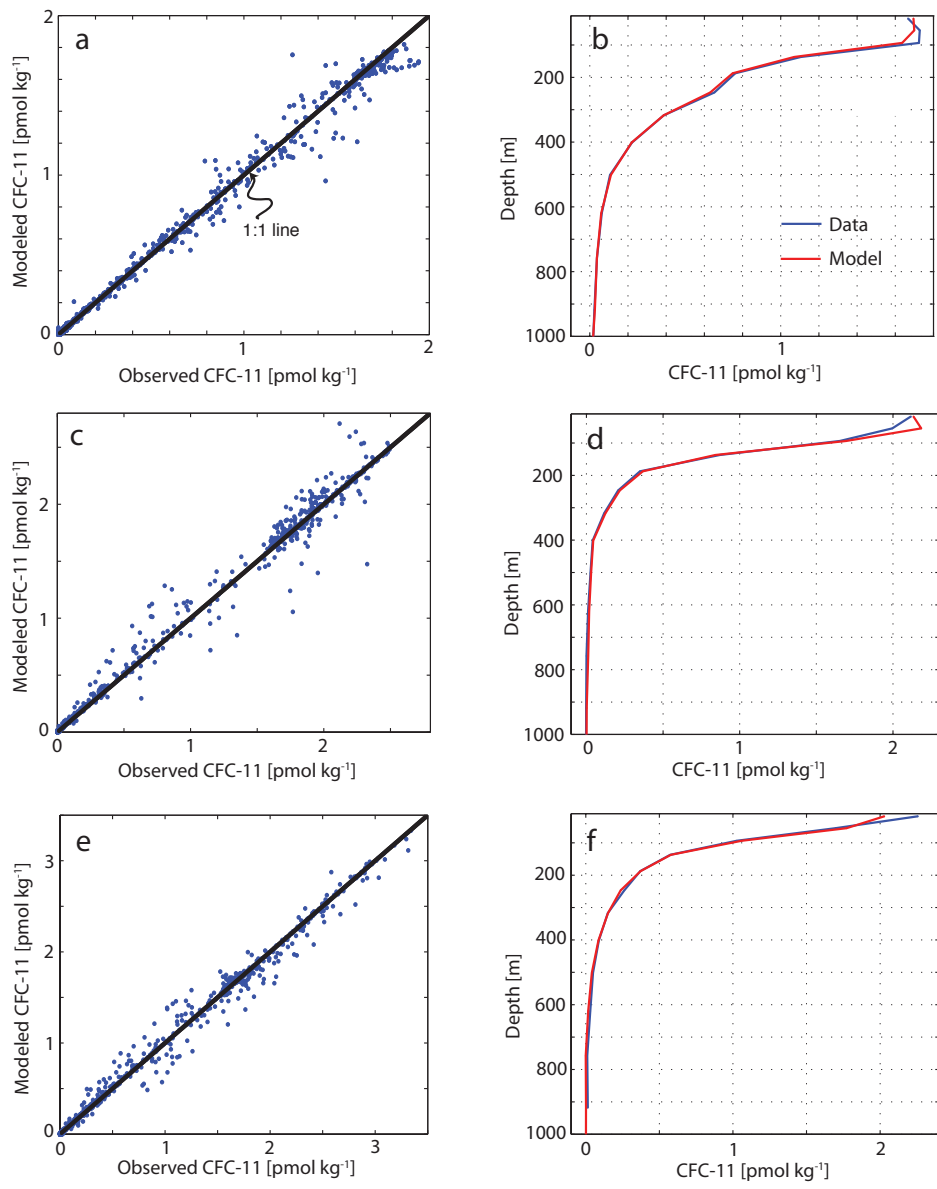
1. DeVries, T. & Primeau, F. Dynamically- and observationally-constrained estimates of water-mass distributions and ages in the global ocean. *J. Phys. Ocean.* (2011).
2. Key, R. M. *et al.* A global ocean carbon climatology: Results from GLODAP. *Glob. Biogeochem. Cycles* **18**, GB4031 (2004).
3. Najjar, R. & Orr, J. Design of OCMIP-2 simulations of chlorofluorocarbons, the solubility pump and common biogeochemistry. online document (1998). <http://www.ipsl/jusiieu.fr/OCMIP/phase2/#simulations>.
4. Wanninkhof, R. Relationship between wind speed and gas exchange over the ocean. *J. Geophys. Res.* **97**, 7373–7382 (1992).
5. Schlitzer, R. Assimilation of Radiocarbon and Chlorofluorocarbon Data to Constrain Deep and Bottom Water Transports in the World Ocean. *J. Phys. Ocean.* **37**, 259–276

- (2007).
6. Ward, B. B. *et al.* Denitrification as the dominant nitrogen loss process in the Arabian Sea. *Nature* **461**, 78–81 (2009).
 7. Lam, P. *et al.* Revising the nitrogen cycle in the peruvian oxygen minimum zone. *Proc. Natl. Acad. Sci.* **106**, 4752–4757 (2009).
 8. Garcia, H. E. *et al.* Volume 3: Dissolved oxygen, apparent oxygen utilization, and oxygen saturation. In Levitus, S. (ed.) *World Ocean Atlas 2009*, 344 pp. (U.S. Government Printing Office, Washington, D.C., 2010).
 9. Bianchi, D., Dunne, J. P., Sarmiento, J. L. & Galbraith, E. D. Global data-based estimates of suboxia, denitrification, and N₂O production in the ocean. *manuscript in prep.* (2011).
 10. Martin, J., Knauer, G., Karl, D. & Broenkow, W. VERTEX: Carbon cycling in the northeast Pacific. *Deep Sea Res.* **34**, 267–285 (1987).
 11. Dunne, J. P., Armstrong, R. A., Gnanadesikan, A. & Sarmiento, J. L. Empirical and mechanistic models for the particle export ratio. *Glob. Biogeochem. Cycles* **19** (2005).
 12. Behrenfeld, M. J. & Falkowski, P. G. Photosynthetic rates derived from satellite-based chlorophyll concentration. *Limn. and Ocean.* **42**, 1–20 (1997).

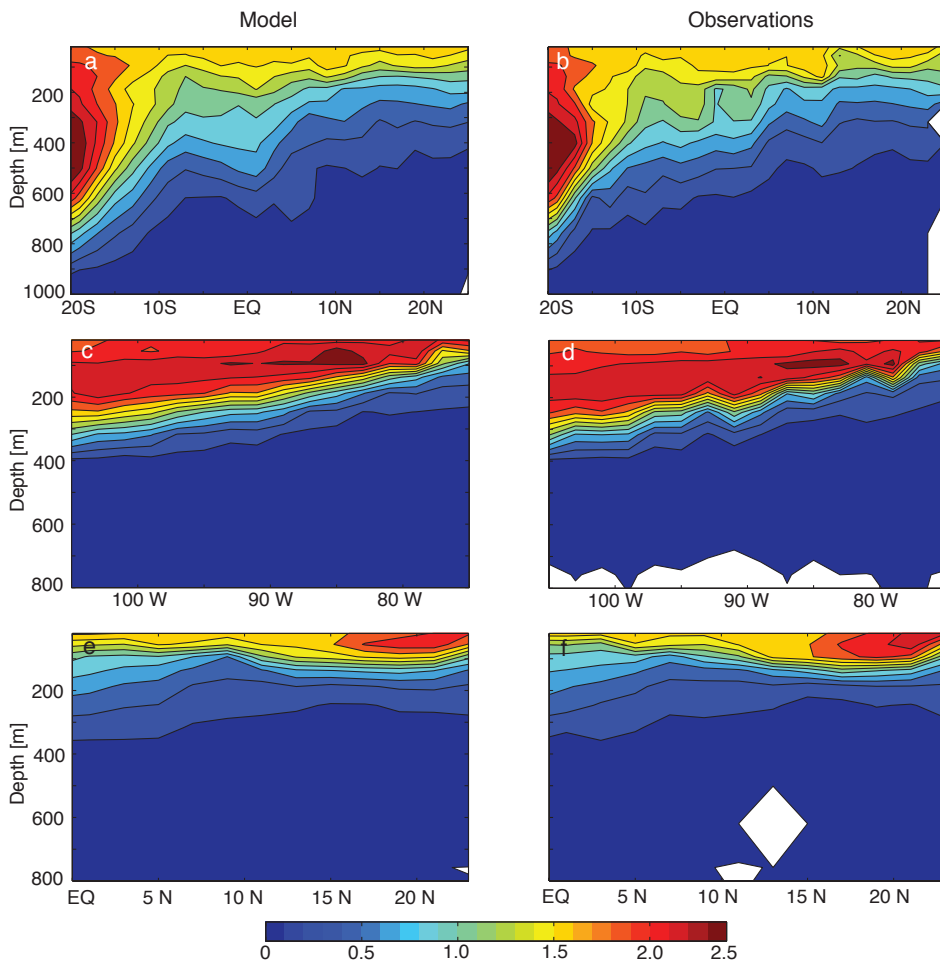
13. Westberry, T., Behrenfeld, M. J., Siegel, D. A. & Boss, E. Carbon-based primary production modeling with vertically resolved photoacclimation. *Glob. Biogeochem. Cycles* **22** (2008).
14. Devol, A. H. *et al.* Denitrification rates and excess nitrogen gas concentrations in the Arabian Sea oxygen deficient zone. *Deep Sea Res. I* **53**, 1533–1547 (2006).
15. Chang, B. X., Devol, A. H. & Emerson, S. R. Denitrification and the nitrogen gas excess in the eastern tropical South Pacific oxygen deficient zone. *Deep Sea Res. I* **57**, 1092–1101 (2010).
16. Chang, B. X., Devol, A. H. & Emerson, S. R. Fixed nitrogen loss from the eastern tropical North Pacific and Arabian Sea oxygen deficient zones determined from measurements of N₂:Ar. *in review* (2011).
17. Paulmier, A., Kriest, I. & Oschlies, A. Stoichiometries of remineralisation and denitrification in global biogeochemical ocean models. *Biogeosciences* **6**, 923–935 (2009).
18. Codispoti, L. A., Yoshinari, T. & Devol, A. H. Suboxic respiration in the oceanic water column. In del Giorgio, P. A. & le B. Williams, P. J. (eds.) *Respiration in Aquatic Ecosystems*, 225–247 (Oxford Univ. Press, New York, 2005).
19. Lutz, M., Dunbar, R. & Caldeira, K. Regional variability in the vertical flux of particulate organic carbon in the ocean interior. *Glob. Biogeochem. Cycles* **16** (2002).

20. Hartnett, H. E. & Devol, A. H. Role of a strong oxygen deficient zone in the preservation and degradation of organic matter: a carbon budget for the continental margins of NW Mexico and Washington State. *Geochim. Cosmochim. Acta* **67**, 247–264 (2003).
21. Mooy, B. A. S. V., Keil, R. G. & Devol, A. H. Impact of suboxia on sinking particulate organic carbon: Enhanced carbon flux and preferential degradation of amino acids via denitrification. *Geochim. Cosmochim. Acta* **66**, 457–465 (2002).
22. Berelson, W. M. The Flux of Particulate Organic Carbon Into the Ocean Interior: A Comparison of Four U.S. JGOFS Regional Studies. *Oceanography* **14**, 59–67 (2001).
23. Neal, R. M. Slice sampling. *Ann. Statist.* **31**, 705–767 (2003).
24. Brooks, S. & Gelman, A. General methods for monitoring convergence of iterative simulations. *Journal of Computational and Graphical Statistics* **7**, 434–455 (1998).
25. Anderson, T. R., Ryabchenko, V. A., Fasham, M. J. R. & Gorchakov, V. A. Denitrification in the arabian sea: A 3d ecosystem modelling study. *Deep-Sea Res. I* **54**, 2082–2119 (2007).
26. Bange, H. W. *et al.* A revised nitrogen budget for the Arabian Sea. *Glob. Biogeochem. Cycles* **14**, 1283–1297 (2000).

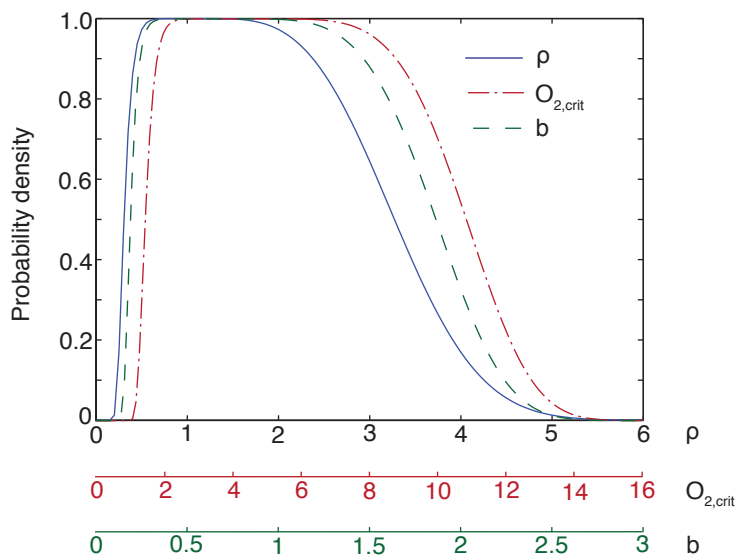
27. Howell, E. A., Doney, S. C., Fine, R. A. & Olson, D. B. Geochemical estimates of denitrification in the Arabian Sea and Bay of Bengal during WOCE. *Geophys. Res. Lett.* **24** (1997).
28. Deutsch, C., Gruber, N., Key, R. M., Sarmiento, J. L. & Ganachaud, A. Denitrification and N₂ fixation in the Pacific Ocean. *Glob. Biogeochem. Cycles* **15**, 483–506 (2001).



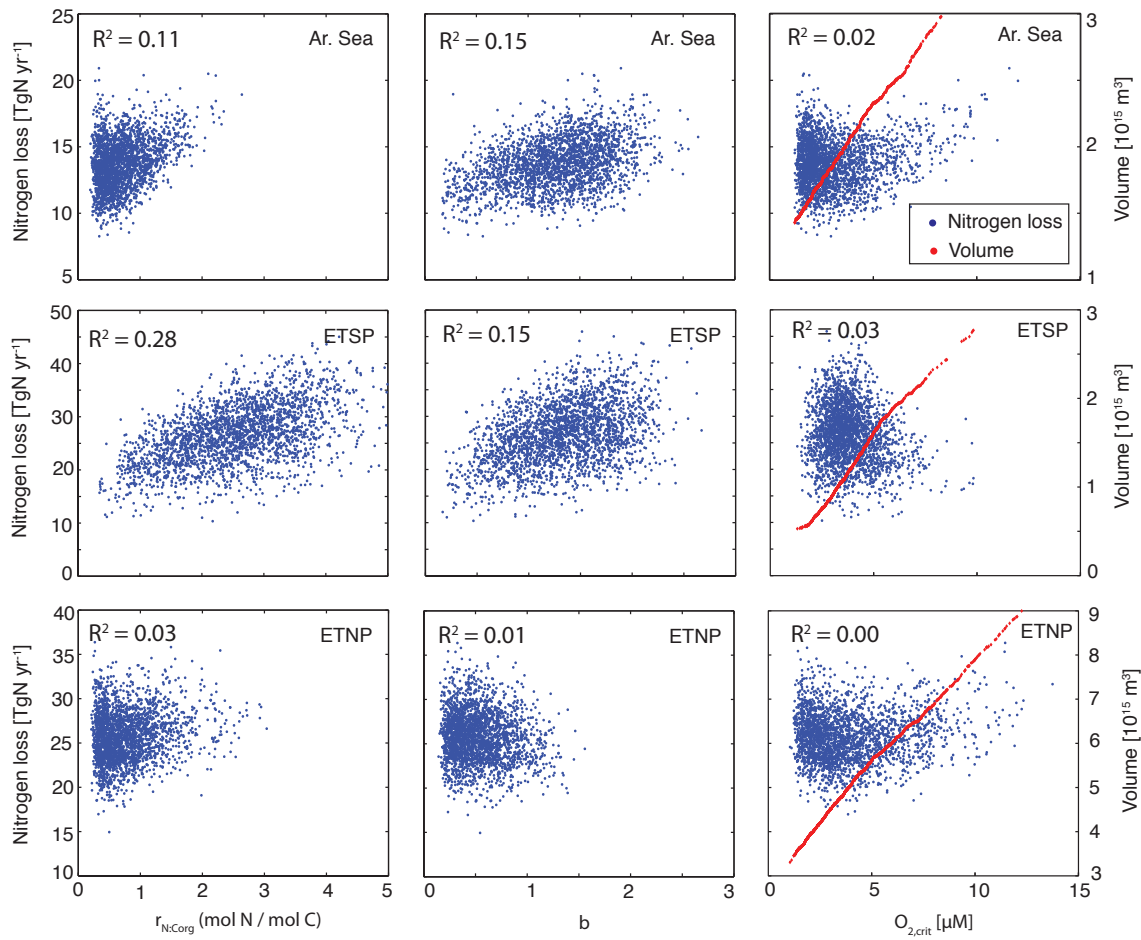
Supplementary Figure 1: Model-data comparison of CFC-11 concentrations. (a-b) the Arabian Sea, (c-d) the ETSP, and (e-f) the ETNP. Observed CFC-11 concentrations are derived from GLODAP bottle data by averaging to the model grid. Depth profiles are averages of CFC-11 concentrations at (19°N, 62-66 °E) in the Arabian Sea, (17°S, 74-
82°W) in the ETSP, and (23°N, 108-112°W) in the ETNP. Data in the Arabian Sea is from 1995, and data in the ETSP and ETNP is from 1994.



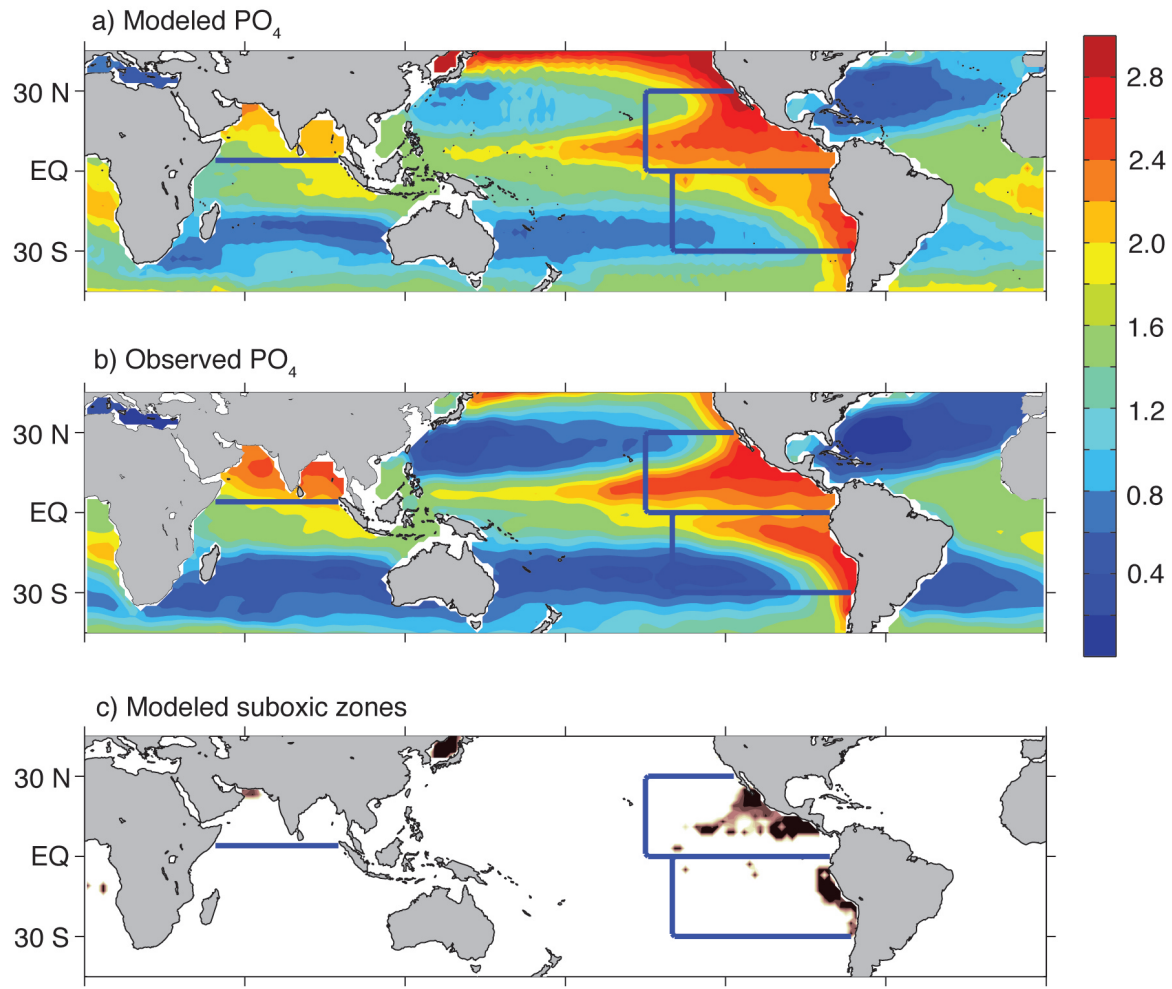
Supplementary Figure 2: Modeled and observed CFC-11 in suboxic zones. Modeled (left panels) and observed (right panels) CFC-11 concentrations along transects through each suboxic zone. (a) and (b) are averages along a quasi-meridional transect through the Arabian Sea from about 50°E to 68°E. (c) and (d) are averages along a zonal transect through the ETSP from 18°S to 14°S. (e) and (f) are averages along a meridional transect through the ETNP from 108°W to 112°W. Contour interval is 0.2 pmol kg⁻¹ in all plots.



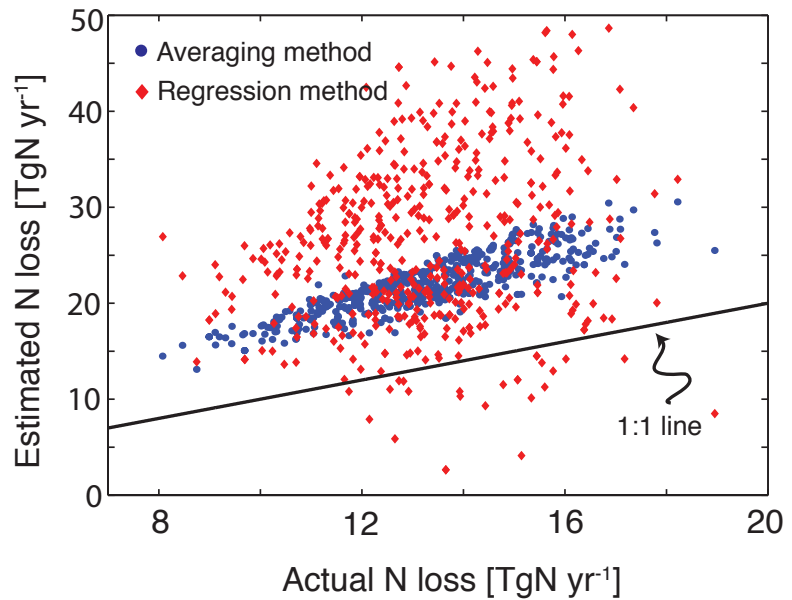
Supplementary Figure 3: Priors for control parameters of the inverse model. Curves have been normalized by the maximum of the pdf.



Supplementary Figure 4: Total nitrogen loss vs. model parameters in each suboxic zone. Each blue dot represents the total N loss in each region from one of 2500 randomly-selected model runs. In the right-hand column, each red dot represents the suboxic volume in each region, showing how the suboxic volume scales with $O_{2,crit}$. When calculating the suboxic volume, the boundary of the suboxic zone is set arbitrarily at $\eta = .01$. R^2 values of a linear fit between integrated N loss and each parameter are given in the upper left-hand corner of each subplot.



Supplementary Figure 5: **Model simulated PO₄ and suboxic zones.** a) Simulated PO₄ distributions from the depth range 150-350 m using an OCMIP-style biogeochemistry model coupled to the data-constrained circulation model. b) Observed PO₄ from the same depth range as panel (a). c) Model simulated extent of the suboxic zones in the Arabian Sea, ETNP, and ETSP, as defined by equation (3) with model-simulated oxygen in place of O_{2,obs} and O_{2,crit} = 5 μ M.



Supplementary Figure 6: N loss estimated by geochemical methods. Total nitrogen loss in the Arabian Sea suboxic zone computed from the model-simulated N_{xs} data using the averaging method and the regression method (see text for description of methods). Numbers on the x -axis are the actual nitrogen loss rates calculated from the model.

Supplementary Table 1: Values of control parameters determined by the MCMC simulations.

	$r_{N:C_{org}}$ ^a	$O_{2,crit}$ ^b	b ^c
Suboxic zone	mol N (molC) ⁻¹	(μ M)	
Arabian Sea	0.7 ± 0.4	3.1 ± 1.6	1.3 ± 0.4
ETSP	2.5 ± 0.9	3.8 ± 1.2	1.4 ± 0.6
ETNP	0.8 ± 0.4	4.0 ± 2.1	0.5 ± 0.3

^a Number of moles N produced as N₂ gas for each mol C remineralized under suboxic conditions

^b Critical oxygen threshold for denitrification

^c Depth attenuation coefficient for organic matter remineralization

Supplementary Table 2: Sensitivity experiments.

Experiment	Integrated N loss (TgN yr^{-1})				Parameter values ^e		
	Global	Arabian Sea	ETSP	ETNP	$r_{N:C_{org}}$	$O_{2,crit}$	b ^f
Standard ^a	66±6	14±2	27±7	26±3	0.7 / 2.5 / 0.8	3.1 / 3.8 / 4.0	1.3 / 1.4 / 0.5
S1 ^b	58±5	14±2	17±4	27±3	1.3 / 2.0 / 1.1	5.7 / 6.0 / 5.2	0.9 / 0.9 / 0.9
S2 ^c	77±7	17±2	30±7	31±3	0.8 / 2.5 / 1.1	3.6 / 3.6 / 4.6	1.1 / 1.4 / 0.6
S3 ^d	72±7	15±2	30±6	28±3	0.8 / 2.5 / 1.1	3.3 / 3.5 / 4.4	1.3 / 1.3 / 0.7

^a As described by equations (2)-(6)

^b Export production parameterized with OCMIP-type model

^c 2X horizontal diffusivity

^d 2X vertical diffusivity

^e The mean value of the posterior pdf for each parameter is given for each experiment, in the order Arabian Sea / ETSP / ETNP. Parameter uncertainty is generally on the order of 50%.

^f The value of b is fixed at 0.9 in Experiment S1.

Supplementary Table 3: Rate of nitrogen loss in the Arabian Sea suboxic zone for five idealized experiments. Rates in TgN yr⁻¹.

Experiment	Actual rate	Rate estimated with	Rate estimated with	Bias
		averaging method	regression method	
1 ^a	13.0	13.0	13.0	None
2 ^b	13.0	16.3	22.8	Positive
3 ^c	13.0	7.5	3.9	Negative
4 ^d	13.0	17.9	20.4	Positive
5 ^e	13.0	22.3	26.1	Positive

^a Uniform boundary condition, uniform production rate

^b Non-uniform boundary condition, uniform production rate

^c Uniform boundary condition, production varies with organic matter remineralization rate

^d Uniform boundary condition, production varies with O₂ concentration

^e Full model: non-uniform boundary condition, production distributed according to equation (4)